

## **Supplementary Material. Mechanism of non-phenolic substrate oxidation by fungal laccase Type 1 Copper site from *Trametes versicolor*. The case of benzo[a]pyrene and anthracene**

Carla Orlando,<sup>a,c</sup> Isabella Cecilia Rizzo,<sup>a</sup> Federica Arrigoni,<sup>a</sup> Jessica Zampolli,<sup>a</sup> Marco Mangiagalli,<sup>a</sup> Patrizia Di Gennaro,<sup>a</sup> Marina Lotti,<sup>a</sup> Luca De Gioia,<sup>a</sup> Tiziana Marino,<sup>c</sup> Claudio Greco,<sup>b</sup> Luca Bertini<sup>a\*</sup>

<sup>a</sup> Department of Biotechnologies and Biosciences, University of Milano-Bicocca, Piazza della Scienza 2, 20126 Milan, Italy. e-mail [luca.bertini@unimib.it](mailto:luca.bertini@unimib.it)

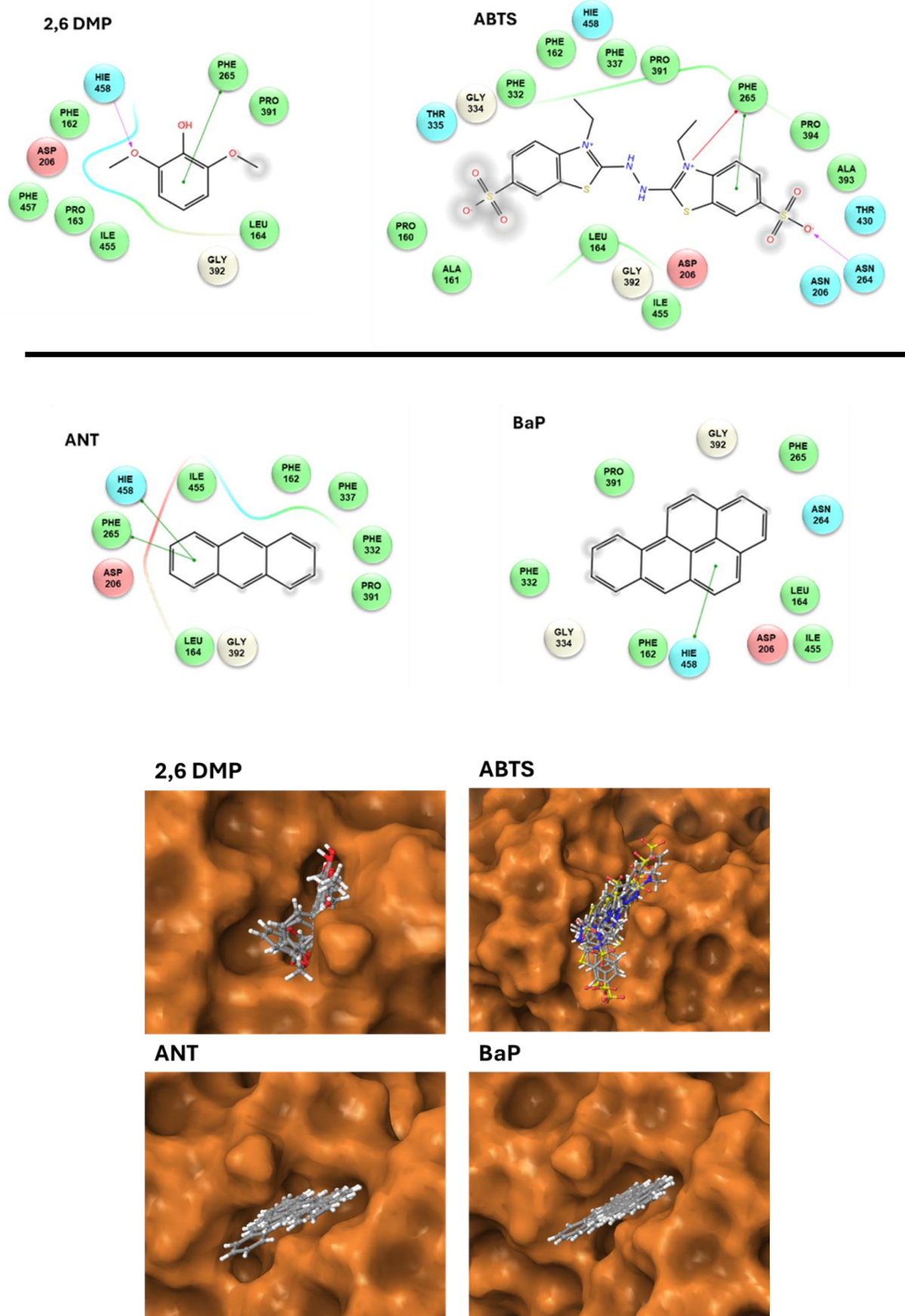
<sup>b</sup> Department of Earth and Environmental Sciences, University of Milano-Bicocca, Milano, Italy

<sup>c</sup> Department of chemistry, Università della Calabria, Rende (CS), Italy

**Table S1.** Summary of docking results for 2,2'-azino-bis(3-ethylbenzothiazoline-6-sulfonic acid (ABTS) and 2,6-dimethoxyphenol (2,6 DMP), Anthracene (ANT) and benzo[a]pyrene (BaP). Distance from T1 has been calculated with respect to the substrate barycenter.

Substrate	Distance from T1 (Å)	H-Bonds	$\pi$ -CAT	$\pi$ - $\pi$	Docking scores (kcal/mol)	Best pose Docking (kcal/mol)
2,6 DMP	3.08	His 458	no	Phe 265	-3.61 / -4.96	-4.96
ABTS	7.07	Asn 264	Phe 265	Phe 265	-3.58 / -4.90	-4.90
ANT	6.78	no	no	His 458 - Phe 265	-2.92 / -3.61	-3.61
BaP	7.20	no	no	His 458	-3.00 / - 4.07	-4.07

**Figure S1.** Interaction diagrams of the best pose obtained for each substrate to TvL. Below are reported the positions of each ligand in the TvL binding pocket.



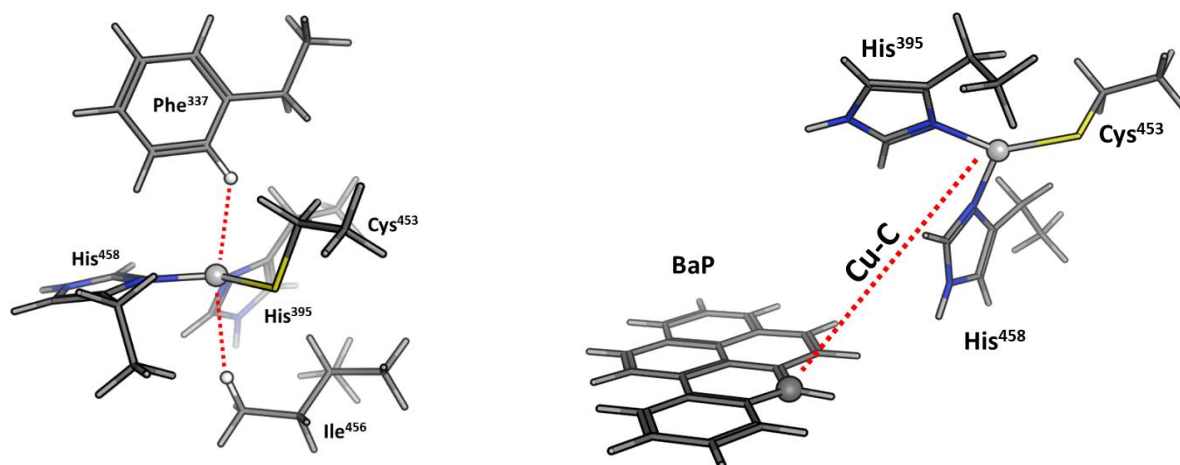


**Table S2.** Large model optimized T1 Cu coordination sphere Cu-ligand bond distances (in Å) for the reactant R-Cu(II) at BP86/TZVP/D3/Cosmo and PBE0/TZVP/D3/Cosmo level of theory; for the Int-Cu(I) at BP86/TZVP/D3/Cosmo. The Cu-H<sub>Phe</sub> and Cu-H<sub>Ile</sub> distances refer to the distances between copper (Cu) and the hydrogen (H) atoms of the side chains of hydrophobic residues, specifically phenylalanine (Phe) and isoleucine (Ile), within the first coordination sphere of T1 copper. These distances are calculated based on the shortest distance between one of the hydrogen atoms within the side chain (see figure above).

	R-Cu(II) ANT		R-Cu(II) BaP		ANT Intermediate Cu(I)	BaP Intermediate Cu(I)
	BP86	PBE0	BP86	PBE0	BP86	BP86
	Cu-N <sub>His</sub>	1.974	1.965	1.972	1.959	1.990
Cu-N <sub>His</sub>	1.975	1.979	1.978	1.976	2.067	2.067
Cu-S <sub>Cys</sub>	2.155	2.142	2.151	2.139	2.192	2.192
Cu-H <sub>Phe</sub>	2.567	2.604	2.630	2.635	2.541	2.539
Cu-H <sub>Ile</sub>	2.708	2.801	2.720	2.824	2.725	2.715
Cu-C	8.210	8.674	8.385	8.614	8.505	8.740

NBO spin population (in electrons) for R-Cu(II) large models computed at BP86 and PBE0 level using optimized BP86/TZVP/D3/Cosmo geometries.

	R-Cu(II)				Int-Cu(I)			
	ANT		BaP		ANT		BaP	
	BP86	PBE0	BP86	PBE0	BP86	PBE0	BP86	PBE0
Cu	0.43	0.50	0.43	0.49	0.12	0.00	0.13	0.00
S <sub>Cys</sub>	0.45	0.43	0.45	0.43	0.08	0.00	0.09	0.00
N <sub>Hi</sub>	0.03	0.03	0.04	0.03	0.00	0.00	0.00	0.00
N <sub>Hi</sub>	0.03	0.03	0.03	0.03	0.00	0.00	0.00	0.00
Ligand	0.00	0.00	0.00	0.00	0.80	1.02	0.75	1.01

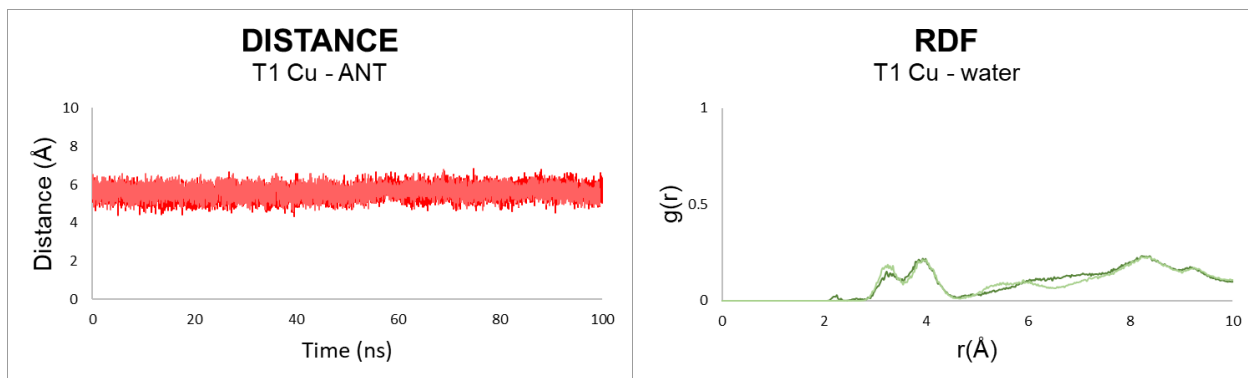


**Figure S2.** Analysis of MD simulations (two replicas) of the enzyme-substrate complex (taking ANT as an example), performed starting from the best docking pose. Left: Distance calculation between ANT and T1 Cu. During both simulations, the substrate maintains essentially the same positioning within the pocket and a distance from T1 Cu similar to the initial conformation. Right: RDF analysis for the T1 Cu and water molecules, calculated for each replica along the entire simulations. This result confirms the presence of water molecules in the first hydration sphere of T1 Cu (2 - 4 Å) in between the metal and the substrate.

MD details: two replicas of 100 ns were performed for the protein in complex with ANT, starting from the best docking pose. By using AmberTools23, the 3D system was placed in a 10 Å cubic box containing a neutralized water buffer with counterions. The system was described by the model from the general Amber force field (GAFF) and ff99SB in combination with the TIP3P water model; proper restraints have been added to maintain a proper coordination in T1 Cu. Using the GROMACS 2020 package *S. Pronk, et al.*, the system was relaxed by applying harmonic positional constraints on all atoms (50 kcal mol<sup>-1</sup> Å<sup>2</sup>) using 5000 steps of steepest descent (SD), followed by 5000 steps of conjugate gradient (CG). The system was progressively heated for 10 ns at 300 K using the Langevin thermostat in the NVT ensemble. The system was maintained at constant pressure with the NPT ensemble at 1 bar pressure using the Berendsen barostat with a time constant  $\tau_p = 2.0$  ps. The 100 ns MDs were produced with an integration step of 2 fs and a cutoff radius of 10.0, with the SHAKE algorithm coupling the Particle Mesh Ewald (PME) summation method. The stability of the complex was verified by monitoring the T1 Cu - ANT distance, calculated with respect to the barycenter of the latter. In order to verify the presence of water molecules in the proximity of T1 Cu, the radial distribution function (RDF) was also calculated.

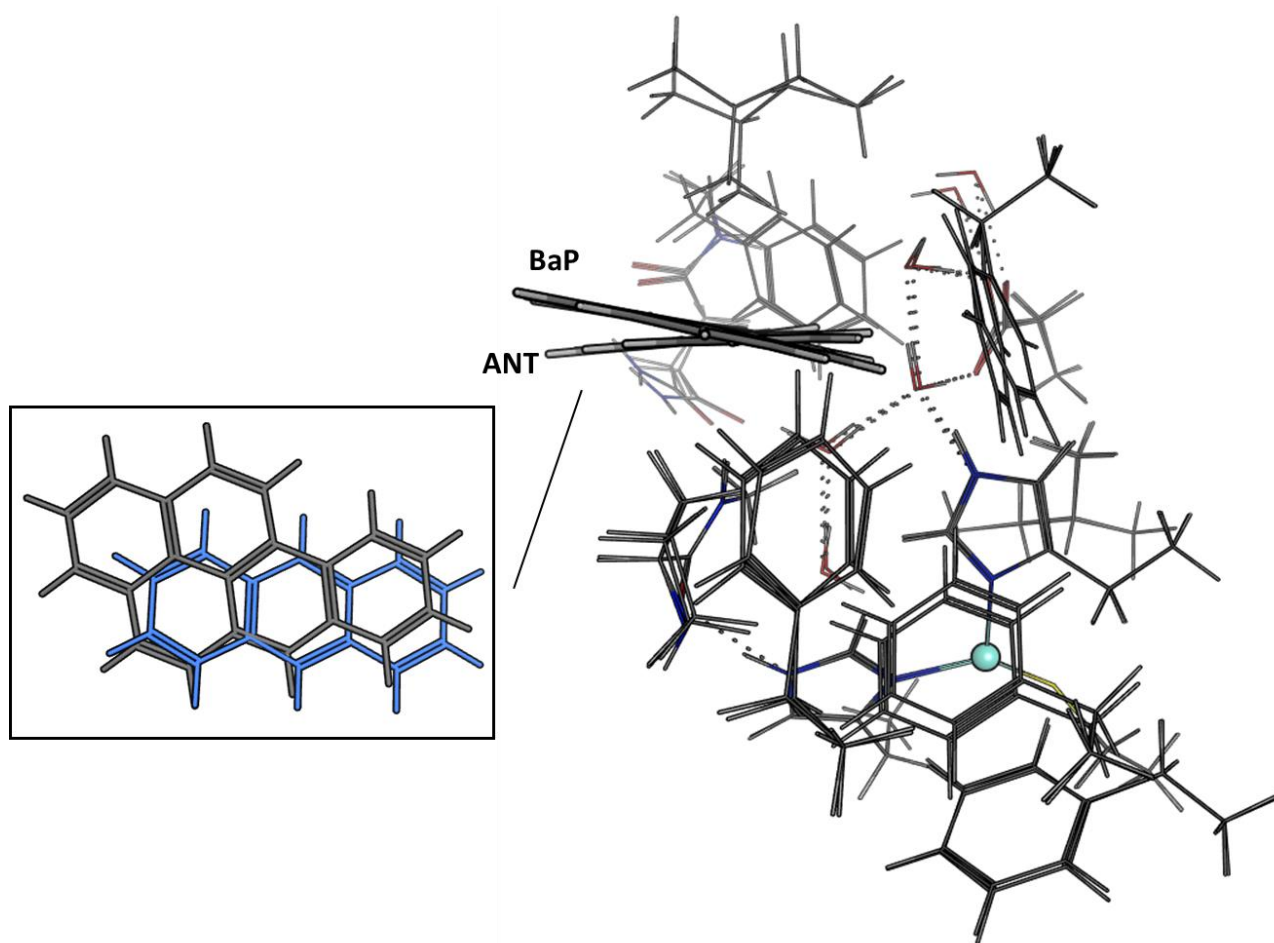


**Figure S3.** Comparison of ANT and BaP geometries, optimized using BP86/TZVP/D3 COSMO  $\epsilon=80$  DFT, within a large cluster model comprising 14 side chain residues ( $C\alpha$  position are fixed at the crystallographic positions from 1KYA pdb), the ligand, and five water molecules. The inset depicts a top view of the ligands, highlighting a slight twisting between the two ligands.

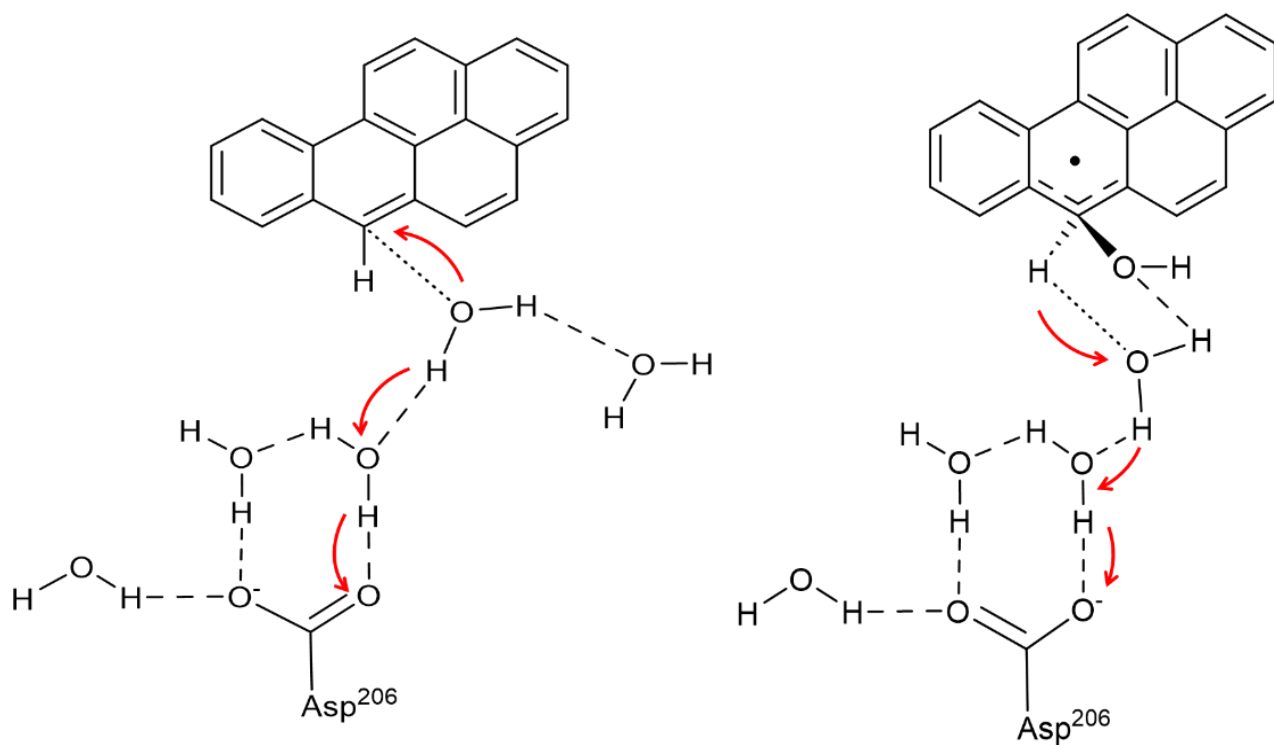


**Figure S4.** Molecular motions along the reaction coordinates for the first (left) and second (right) oxidation steps of BaP. The observed atomic displacements in BaP are equally observed in ANT. The dotted line indicates the interatomic distance explored in the PES scan. The red arrows indicate the atomic displacements observed during the PES scan.

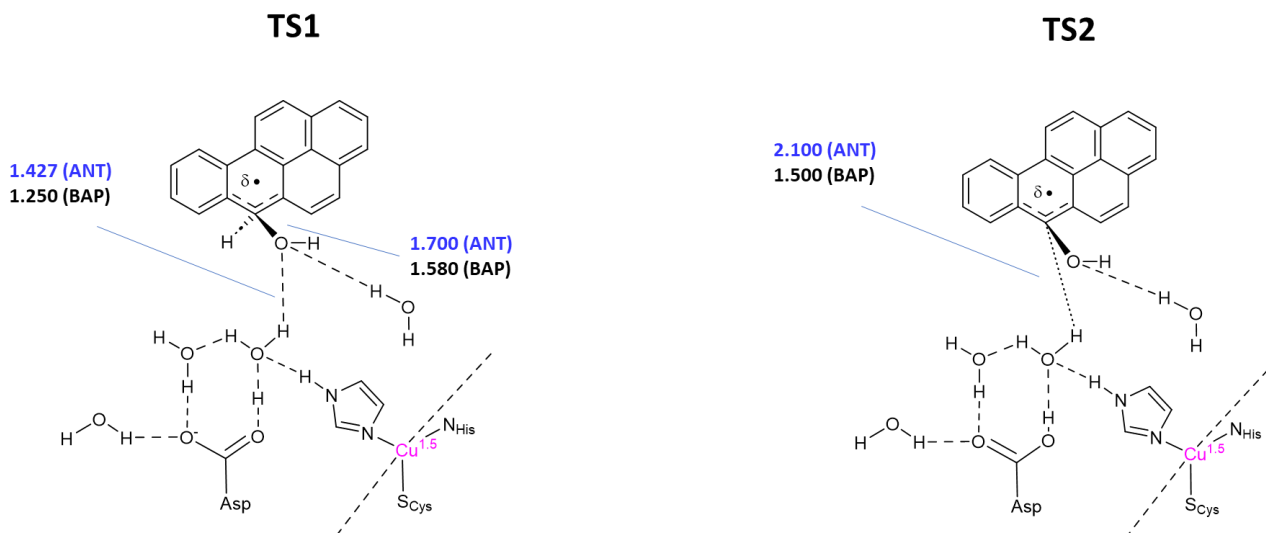


**Figure S5.** Geometries of the first and second transition state (TS1 and TS2) along the reaction coordinates for the first and second oxidation steps. In both cases the NBO spin population computed at PBE0/TZVP/D3 COSMO  $\Sigma=80$  DFT level of the copper ion is compatible with the  $\text{Cu}^{1.5}$  redox state. In the case of TS1 for BaP, a spin population of 0.6 is observed on the ligand, indicating that Cu is slightly more reduced compared to ANT.



**Table S3.** Transition state Cu-X (in Å) optimized bond distances at BP86/TZVP/D3/COSMO level.

	<b>TS1</b>		<b>TS2</b>	
	<b>ANT</b>	<b>BaP</b>	<b>ANT</b>	<b>BaP</b>
Cu-N <sub>His</sub>	2.002	1.996	2.001	1.972
Cu-N <sub>His</sub>	2.007	2.047	2.017	1.977
Cu-S <sub>Cys</sub>	2.184	2.193	2.186	2.156
Cu-H <sub>Phe</sub>	2.594	2.630	2.532	2.608
Cu-H <sub>Ile</sub>	2.702	2.814	2.612	2.673

**Table S4.** Reaction energy barriers (in kcal/mol) computed at BP86/TZVP/D3/Cosmo level and PBE0/TZVP/D3/Cosmo level from BP86/TZVP/D3/Cosmo level optimized geometries.  $\otimes E_1^\#$  and  $\otimes E_2^\#$  are the energy barrier between the R-Cu(II) and Int-Cu(I) ( $\otimes E_1^\#$ ) and between Int-Cu(II)/P-Cu(I).

Level of theory	BP86 TZVP/D3/Cosmo		PBE0 TZVP/D3/Cosmo	
	ANT	BaP	ANT	BaP
$\otimes E_1^\#$	31.1	29.1	29.7	30.3
$\otimes E_{r,1ox}$	26.4	20.1	18.1	14.8
$\otimes E_2^\#$	19.3	28.1	27.9	30.5
$\otimes E_{r,2ox}$	-48.8	-31.7	-46.8	-27.5

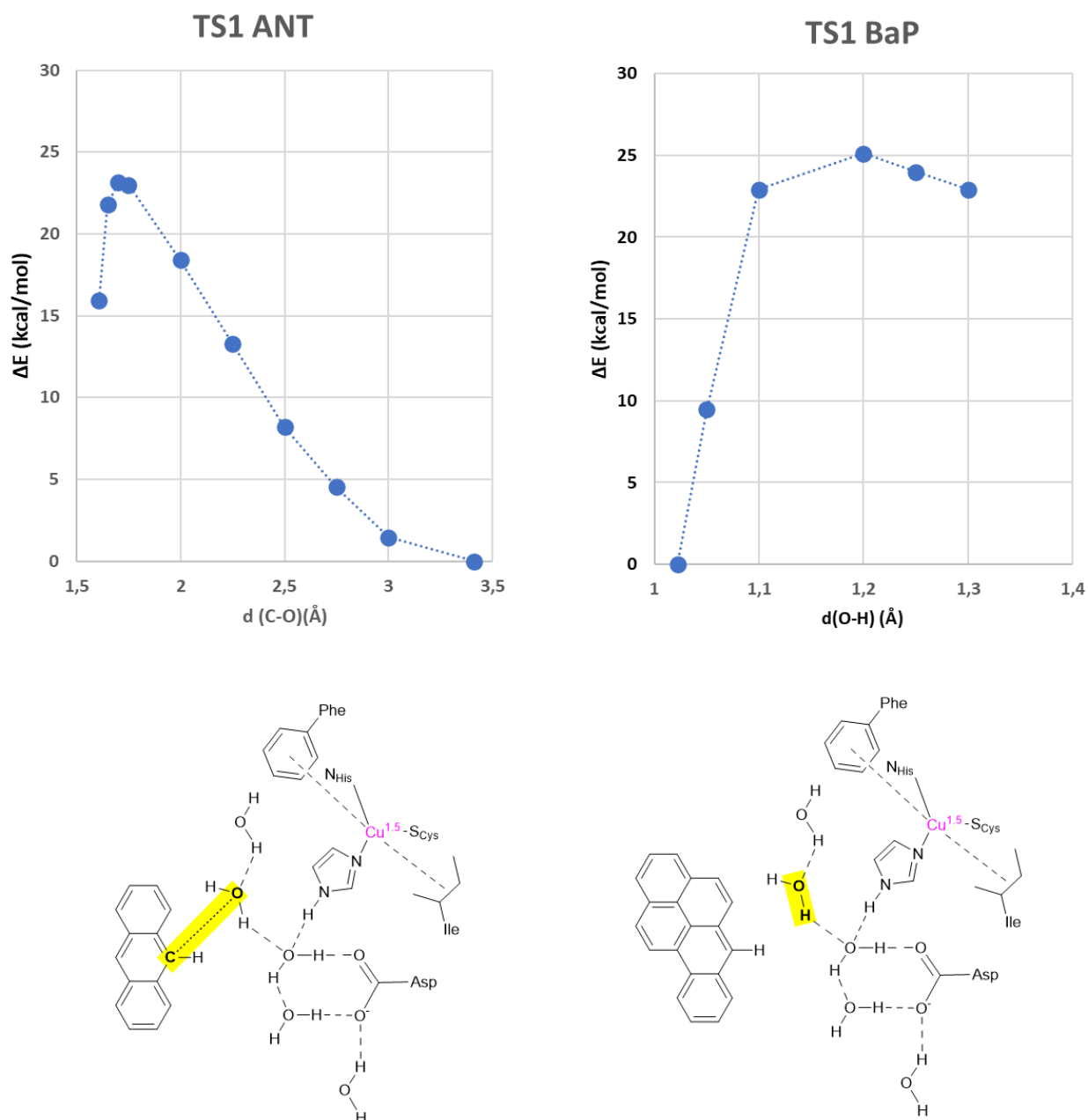


**Figure S6.** Potential energy surface scans along the reaction coordinate for the first oxidation step at BP86/SV-P/D3/COSMO level. The interatomic distances evidenced in yellow are those considered to implement the energy scan. In the main text are then reported the energy barrier of the transition state structure obtained from these scans upon re-optimization at BP86/TZVP/D3 COSMO level and single-point energy calculation at PBE0/TZVP/D3 COSMO level on BP86/TZVP/D3/COSMO optimized saddle points.

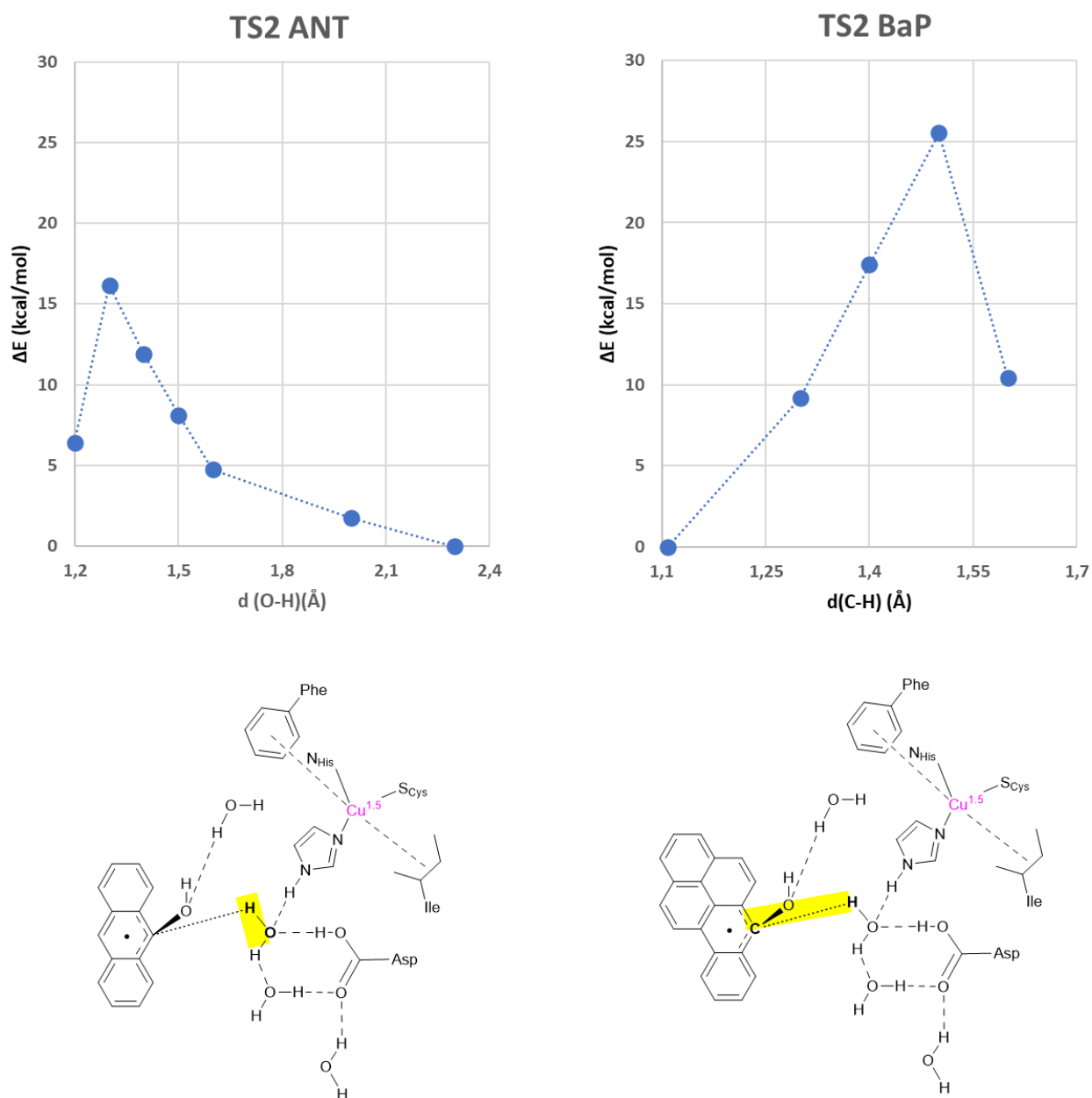


**Figure S7.** Potential energy surface scans along the reaction coordinate for the second oxidation step at BP86/SV-P/D3/COSMO level. The interatomic distances evidenced in yellow are those considered to implement the energy scan. In the main text are then reported the energy barrier of the transition state structure obtained from these scans upon re-optimization at BP86/TZVP/D3 COSMO level and single-point energy calculation at PBE0/TZVP/D3 COSMO level on BP86/TZVP/D3/COSMO optimized saddle points.

**Table S5.** Summary of the ANT and BaP oxidation experiment with fungal laccases in absence of mediator. % ox refers to the percentage of oxidized quinone product with respect to the control without enzyme.

Organism	Experimental condition with no mediator	% ox ANT	% ox BaP	Reference
<i>Trametes versicolor</i>	27 °C, pH=5, Tween80, 24h	85%	<2%	(Collins et al. 1996)
<i>Trametes versicolor</i>	pH 5.0, RT, 72h	18%	19%	(Majcherczyk, Johannes, and Hüttermann 1998)
<i>Marasmius quercophilus</i>	pH 4.5	30%		(Farnet et al. 2009)
<i>Trametes versicolor</i>	pH 4.5, Tween80	73.8%	5.3%	(Johannes and Majcherczyk 2000)
<i>Pycnoporus cinnabarinus</i>	pH 5, Tween80	65%		(Cañas et al. 2007)
<i>Trametes versicolor</i>	Immobilized enzyme, pH 4.5, Tween80	17%	19%	(Dodor, Hwang, and Ekunwe 2004)
<i>Rigidoporus lignosus</i>	pH 4.5, 30°C, 72h	9%		(Cambria et al. 2008)
<i>Pleurotus ostreatus D1</i>	pH 4.5	0%		(Natalia N. Pozdnyakova et al. 2006)
yellow laccase from <i>Pleurotus ostreatus D1</i>	pH 6, Tween80	95%		(N. N. Pozdnyakova, Rodakiewicz-Nowak, and Turkovskaya 2004)

## References

- M. T. Cambria, Z. Minniti, V. Librando, and A. Cambria. 2008. **“Degradation of Polycyclic Aromatic Hydrocarbons by Rigidoporus Lignosus and Its Laccase in the Presence of Redox Mediators.”** *Applied Biochemistry and Biotechnology* 149 (1): 1–8.
- A. I. Cañas, M. Alcalde, F. Plou, M. J. Martínez, A. T. Martínez, and S. Camarero. 2007. **“Transformation of Polycyclic Aromatic Hydrocarbons by Laccase Is Strongly Enhanced by Phenolic Compounds Present in Soil.”** *Environmental Science & Technology* 41 (8): 2964–71.
- P. J. Collins, M. Kotterman, J. A. Field, and A. Dobson. 1996. **“Oxidation of Anthracene and Benzo[a]pyrene by Laccases from Trametes Versicolor.”** *Applied and Environmental Microbiology* 62 (12): 4563–67.
- D. E. Dodor, H. Hwang, and S. I. Ekunwe. 2004. **“Oxidation of Anthracene and Benzo[a]pyrene by Immobilized Laccase from Trametes Versicolor.”** *Enzyme and Microbial Technology* 35 (2-3): 210–17.
- A. M. Farnet, G. Gil, F. Ruaudel, A. C. Chevremont, and E. Ferre. 2009. **“Polycyclic Aromatic Hydrocarbon Transformation with Laccases of a White-Rot Fungus Isolated from a Mediterranean Schlerophyllous Litter.”** *Geoderma* 149 (3-4): 267–71.
- C. Johannes, and A. Majcherczyk. 2000. **“Natural Mediators in the Oxidation of Polycyclic Aromatic Hydrocarbons by Laccase Mediator Systems.”** *Applied and Environmental Microbiology* 66 (2): 524–28.
- A. Majcherczyk, C. Johannes, and A. Hüttermann. 1998. **“Oxidation of Polycyclic Aromatic Hydrocarbons (PAH) by Laccase of Trametes Versicolor.”** *Enzyme and Microbial Technology* 22 (5): 335–41.
- N. N. Pozdnyakova, J. Rodakiewicz-Nowak, O. V. Turkovskaya, and J. Haber. 2006. **“Oxidative Degradation of Polyaromatic Hydrocarbons Catalyzed by Blue Laccase from Pleurotus Ostreatus D1 in the Presence of Synthetic Mediators.”** *Enzyme and Microbial Technology* 39 (6): 1242–49.
- N. N. Pozdnyakova, J. Rodakiewicz-Nowak, and O. V. Turkovskaya. 2004. **“Catalytic Properties of Yellow Laccase from Pleurotus Ostreatus D1.”** *Journal of Molecular Catalysis. B, Enzymatic* 30 (1): 19–24.
- S. Pronk, S. Páll, R. Schulz, P. Larsson, P. Bjelkmar, R. Apostolov, M. R. Shirts, J. C. Smith, P. M. Kasson, D. van der Spoel, B. Hess and E. Lindahl. 2013. **“GROMACS 4.5: a high-throughput and highly parallel open source molecular simulation toolkit.”** *Bioinformatics*, 29 (7): 845–854.















-59.51925947900433	4.96270370079323	95.51057106788950	h	-64.03806913113742	5.66937008802219	104.60583844363774	c
-59.67997220326512	8.21080628395692	94.71976019555633	h	-56.10138386204327	10.11630199145001	103.89955628633592	h
-56.73516203030005	11.21972976169152	96.60487981479721	h	-55.52782897787016	6.00194754424970	107.07817445669914	h
-55.53598970180143	3.22547442271348	97.57894185690209	h	-61.73719063217501	16.19944384552399	116.15277712920501	h
-53.44930758586070	12.10604660763785	99.82766563318218	h	-66.35757239013424	15.92697235774350	117.02529107164631	h
-52.31583480065415	4.08402388261072	100.85211525815227	h	-69.13082556069725	13.28035672737986	114.31373130432053	h
-51.30115107457425	8.53634701434320	102.06212980396130	h	-69.60077658025816	10.13124651428923	110.82998050485689	h
-56.29063794217964	7.59368295698777	91.45571004954452	h	-67.72965324681330	7.59761949174764	107.45694637007796	h
-62.95986630919904	15.06221954632734	114.94162514849846	c	-56.29557156665784	13.1678819305117	109.67836687974568	h
-65.55648642736320	14.90715629292051	115.42373132379532	c	-58.03071564820971	15.05722962898971	113.54019729354198	h
-67.11335004841553	13.42464077233311	113.90760037719659	c	-57.20684102652910	7.22855680420051	102.41549012783024	h
-66.09511098428355	12.00314520489506	111.88529074940774	c	-59.51694433819632	3.84955435096691	100.38785096840691	h
-67.58870085108052	10.30781006334064	110.40867490374679	c	-63.94005945682900	2.77960113290389	101.75974777229196	h
-66.52508639313493	8.88876121456657	108.51653712192727	c	-65.94920469470951	5.16514623713373	105.18132706472262	h
-63.91146980415754	9.10821399099856	107.86855492062602	c	-52.10901571129142	11.46466305214082	108.53019312929295	o
-62.75889189447098	7.66453127575592	105.86570345921149	c	-52.77391249438102	13.01924435118496	107.63572742093353	h
-60.21832681060054	8.24266330505850	105.08451705923729	c	-54.88502389343421	14.96270145024633	104.97881859728285	h
-58.87697465551225	10.23154217458022	106.32120983317355	c	-53.30200665088089	15.45871666781683	105.78280402259122	o
-56.58692018642522	11.05862153403463	105.41894046108587	o	-51.94367572418000	14.87674801993534	104.61961815980170	h
-59.80156626417336	11.32990954155109	108.53774152731664	c	-50.45230051850896	15.77522542556258	98.58277466431032	o
-58.27772724968220	12.89744856781642	110.14810227852254	c	-49.84404296701059	14.91994763550073	100.12487994112180	h
-59.24581674870507	13.96795864589591	112.28495498269126	c	-51.59440512699025	17.07495215999868	99.20237088814994	h
-61.88448577185398	13.76603049481741	112.8905811668761	c	-54.13754236625184	6.80710682365606	107.97365150817467	o
-63.45669775548309	12.21731036315180	111.32212924646377	c	-53.22112668702724	10.02543851965246	108.05609117346182	h
-62.39264746321902	10.84632192455277	109.24549037096737	c	-52.84384251142457	5.50899744401587	108.14628305076735	h
-59.11693242989159	6.82526845951482	103.08404689765241	c				
-60.42314002761066	4.89690583869669	101.91245387911937	c				
-62.90962574375528	4.31006392108639	102.67875679307562	c				